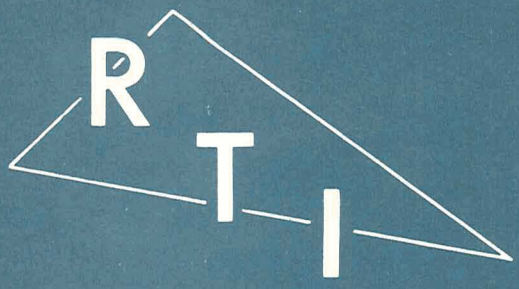

RESEARCH TRIANGLE INSTITUTE

NASA CR-111953

STUDY OF CONDUCTION OF METALLIC LAYERS IMPLANTED IN AMORPHOUS LAYERS

R. P. Donovan
Research Triangle Institute
Research Triangle Park, North Carolina

September 1971

Prepared under Contract No. NAS1-9996 by
RESEARCH TRIANGLE INSTITUTE
RESEARCH TRIANGLE PARK, NORTH CAROLINA

for Langley Research Center

NATIONAL AERONAUTICS AND SPACE ADMINISTRATION

FOREWORD

The experiments to be described in this report were sponsored by the Instrument Techniques Section of NASA Langley Research Center, Hampton, Virginia as a cooperative research effort between Langley and Research Triangle Institute. Mr. H. D. Hendricks was the chief Langley participant; Mr. R. P. Donovan, the chief RTI participant. The research began in May 1970 and ended in July 1971.

It is a pleasure to thank Mr. J. H. Siviter of the Meteoroid Research Section of Space Technology Division, NASA Langley Research Center, for providing us with various low temperature, gold wire bonds during the course of the program.

ABSTRACT

The purpose of this contract was to study the electrical properties of metallic layers implanted into amorphous oxide glass. The glass substrates used throughout the investigation were thick layers of oxide thermally grown on polished silicon substrates. The reason for choosing such a substrate is the good reproducibility of the oxide films formed by this method which capitalizes on the well developed planar technology of contemporary silicon devices.

The primary property measured in evaluating the implanted layers was electrical conductivity. The conductivity of the implanted metallic layer can in principle differ by multiple orders of magnitude from that of the host lattice of the insulating oxide. Consequently this parameter is expected to be a sensitive measure of any modification in the glass brought about by the implantation process. In addition the simple conductive resistor structures formed can have practical applications of their own.

Results of the investigation carried out under this program have not identified any conduction attributed to the implanted metallic layer. Resistors of various magnitudes and temperature coefficient have been measured but these have been the properties of other conducting paths rather than the properties of the implanted layer. The extraneous conducting paths which dominate the measurements included:

(1) A surface deposit resulting from exposure of the oxidized silicon to the implanting beam (this film could be removed by an oxygen plasma cleaning step similar to those becoming popular for the removal of photoresist films);

(2) A path defined by aluminum penetration through the oxide to the underlying silicon (this path was negligible until the annealing temperature exceeded 550°C).

The failure to observe electrical conductivity caused by implantation at the fluences and energies employed suggests that one or more of the assumptions of the experiment are invalid. Possible explanations include:

(1) The LSS model for implantation of these ions into oxide may not be adequate for predicting their final position. Diffusion effects might reduce the peak concentration of the implanted beam from that predicted or precipitation effects may upset the assumed lateral uniformity of the implanted layer. Profiling experiments and analysis with transmission electron microscopy are recommended to aid in understanding the lack of conductivity.

(2) The assumption that the implanted species does not interact with the host SiO_2 may be erroneous.

Reordering after implantation could easily result in the formation of ternary compounds similar to those used in ceramics. These compounds are insulators and would not be detected by the measuring methods employed here. Their presence should be detectable by electron diffraction, IR absorption or other structure-sensitive measures.

TABLE OF CONTENTS

LIST OF ILLUSTRATIONS

LIST OF TABLES

SECTION I

BACKGROUND

The ideas on which this research was based involve the basic concepts of the structure of solids. The molecules or atoms of a solid are held together by either covalent bonds or by ionic forces. Glasses and thermal oxides on silicon are primarily covalently bonded tetrahedra of silicon and oxygen atoms which form a relatively stable SiO_2 complex. The tetrahedra themselves can be ordered or disordered as illustrated in Fig. 1 to form a glassy or a crystalline solid.

A key assumption of this work is that one can implant a metallic species into the existing SiO_2 network and treat the resulting structure as an imbedded collection of hydrogen-like atoms within the previously existing SiO_2 network. Since many of the covalent SiO_2 bonds will be broken during the implantation process, at least in the vicinity of maximum energy loss by the implanted beam, this assumption implies that the original SiO_2 structure will regrow without incorporating the newly

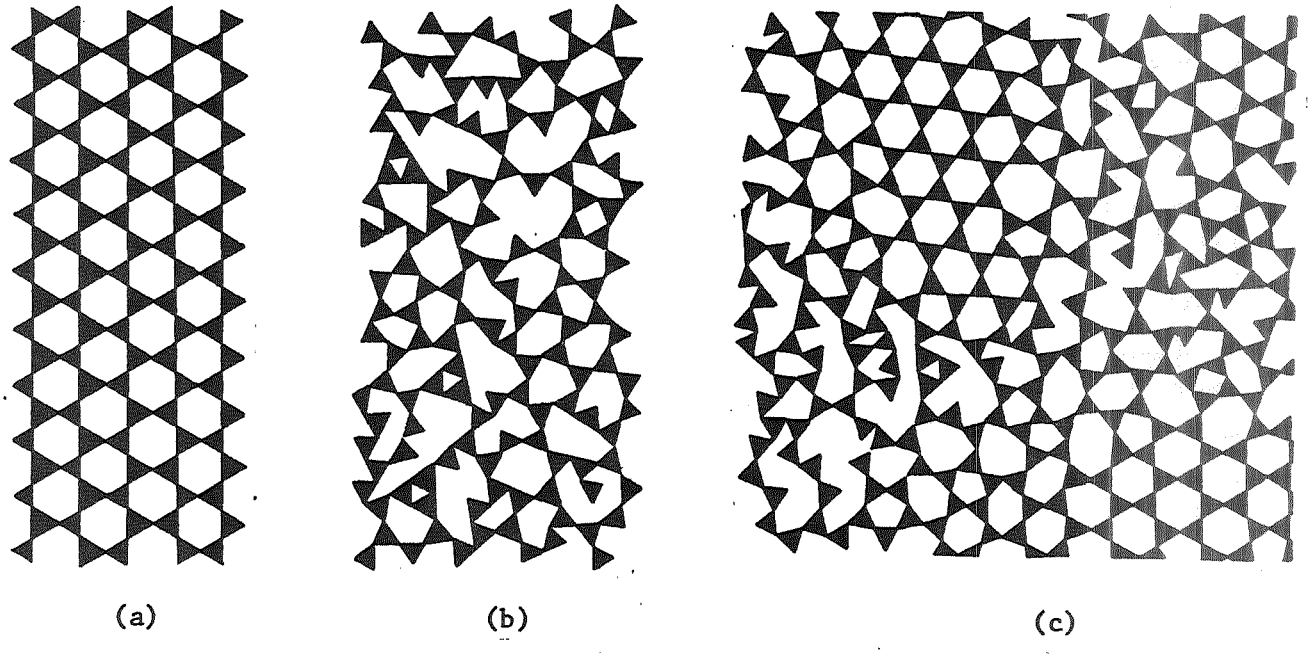

Fig. 1. Two dimensional schematics of: (a) silica crystal network, (b) silica glass network as described by Zachariasen, and (c) silica glass viewed as a polymer-crystalline network.

implanted metallic species in any significant degree. If this assumption is valid, then the properties of the implanted layer should be consistent with a model in which the implanted species do not interact with the SiO_2 lattice and no new chemical species are formed (such as Al_2O_3, MgO, or a ternary compound of silicon, oxygen, aluminum or magnesium). The properties of the implanted layer are expected to vary with the distance between nearest neighbor implanted metal atoms, which in turn is determined by the dose of the implantation process. If any compound forms or if the covalent bound structure of the implanted region changes, then knowledge of this new structure is probably necessary before electrical behavior can be predicted even qualitatively. Most likely the assumption of no interaction between the implanted species and the substrate lattice is valid only for certain species. The species chosen for investigation in this program were selected so as to have a variety of anticipated interactions between the implanted atom and the substrate lattice.

Predicted Profile of Implanted Species

The impurity profile assumed to characterize the implanted layers is the Gaussian distribution predicted by Lindhard, Scharff and Schiott (LSS) [Ref. 1]. The interaction problem solved by LSS is that of a series of two-body Rutherford scattering events. Multiple collisions are handled by summing separate, successive collisions, the incident particle for the i^{th} collision being the scattered particle from the i^{th}-1 collision. The consequences of this model and the resultant distributions have been reviewed by Gibbons [Ref. 2] and a program has been written to facilitate computations based on this model [Ref. 3]. The values calculated in Ref. 3 are those used in predicting the distributions and concentrations for the work performed here. Reference 3 tabulates various ranges and range scatterings for different species into SiO_2. Energy of implantation is a parameter in the tabulations. Consequently, one can calculate the Gaussian profile for any given implantation energy by using the values of mean projected range, $\bar{R}_p$, and range straggling, $\Delta\bar{R}_p$, listed in Ref. 3. Using these values in Eqs. (1) and (2), a plot of the impurity profiles such as shown in Fig. 2 can be constructed.

Peak concentration is given by:

$$N_{max} = \frac{0.4 \text{ (fluence)}}{\overline{\Delta R}_p} \qquad (1)$$

where N_{max} is the maximum impurity concentration which occurs at a depth of $\bar{R}_p$.

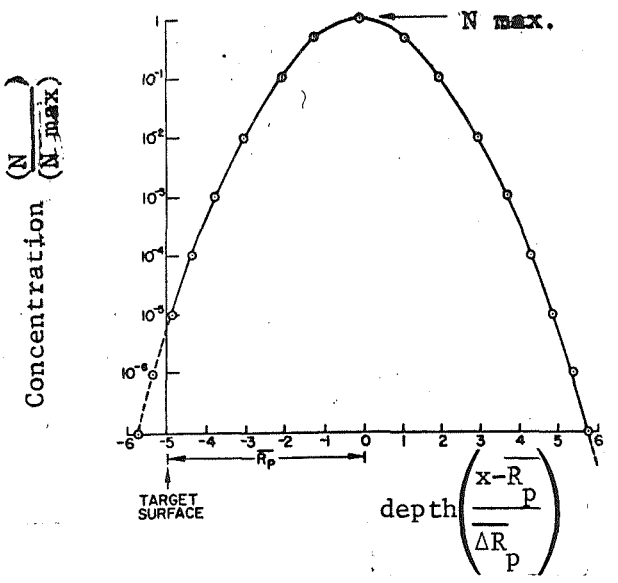

Fig. 2. Gaussian impurity profile for ions implanted into an amorphous target [Ref. 2]

Concentration as a function of depth is predicted to be:

$$N(x) = N_{max} \exp\left[-\frac{1}{2}\left(\frac{x-\bar{R}_p}{\overline{\Delta R}_p}\right)^2\right] \qquad (2)$$

where x is depth expressed in terms of $\bar{R}_p \pm \overline{\Delta R}_p$.

This model neglects any influence of substrate structure upon the predicted impurity profile; it ignores any post-implantation diffusion or impurity motion at thermal energy. The neglect of substrate structure is well justified in the case of an amorphous thermal oxide on silicon; the neglect of additional impurity motion following implantation may be more questionable.

Conduction Mechanisms

The contribution of the implanted metal ions to the conductivity of the implanted layer depends upon the spacing between nearest neighbor metal atoms. Conduction varies from the case in which the nearest neighbor spacing is so great that no appreciable interaction between nearest neighbor implanted metal atoms exists to the case in which the nearest neighbor metal atoms are so close that metallic conduction occurs because

of electron orbit overlap between nearest neighbor atoms. Between these two extremes are the cases of restricted carrier transport between nearest neighbors including tunnelling and hopping. The temperature dependence of each of these processes differs from the other and hence conductivity measurements as a function of temperature are a simple means of distinguishing between them.

Semiconductors exhibit conductivity which increases with temperature and is characterized by an activation energy. This means that the resistivity increases exponentially with increasing reciprocal, absolute temperature (T). The slope of a plot of resistivity versus 1/T gives the magnitude of the activation energy. Metals, on the other hand, are characterized by an increasing resistivity with temperature. The explanation in the simple band model is that the resistivity of a semiconductor is dominated by increasing carrier concentration with temperature while the metal experiences no changing carrier concentration with increasing temperature but rather increased scattering and hence a reduced carrier mobility. Consequently, not only the magnitude of the conductivity of an implanted layer is important, but in particular a measure of the temperature dependence of the conduction layer is valuable in interpreting the electrical properties of the implanted layer.

Sputtering

A further assumption of this experiment is that the results will not be sputter limited. Implantation at high fluence can encounter a sputter limit condition in which the flux of dopant ions (previously implanted by the ion beam) sputtered from the sample surface equals the dopant flux in the primary ion beam. Once this condition is reached no further increase in implanted ion density can occur. Losses due to sputtering depend upon the sputtering yield (the number of sputtered atoms per incident ion) which in turn is energy dependent and the mean projected range of the implanted ion which is also energy dependent. Implantations above 100 keV generally reduce sputtering losses to small or negligible levels.

SECTION II

EXPERIMENTAL

This section describes the sample preparation, the implantation procedures and the measurements made in evaluation. Each of these topics is discussed in the following subsections.

Sample Preparation

10 Ω cm, P-type silicon, oriented in a <100> direction was used throughout as the substrate for growing thick, thermal oxides which acted as the host-glass matrix into which the metal layers were implanted. Typically the oxide layers were 2 μm thick and were prepared by steam oxidation at 1100°C for sixteen (16) hours.

Following the formation of the thick oxide layer the entire surface was coated with 1 μm of evaporated aluminum. By standard photoengraving methods, the aluminum was substractively etched to leave a pattern of concentric rings on the surface. The dimensions and appearance of these rings are shown in Fig. 3. These rings served both as a mask during the implantation and as a contact to the implanted layer following the implantation.

Using the aluminum rings as a contact assumes that the etched border of the aluminum ring is a tapered wedge. This assumption was checked by scanning electron microscopy; the uniformity of the etch and the dimensions involved for this particular etch show the taper of the edge of the aluminum to make an angle of about 4° with the oxide surface. This angle is shallow enough to produce a gradual outcropping of the implanted layer which mirrors the wedge at the surface as schematically illustrated in Fig. 4. The assumption is that the depth to which the beam penetrates on the average ($\bar{R}_p$) transitions from that depth in the unmasked region of the oxide up to the aluminum ring as shown in Fig. 4. Consequently, the aluminum ring is connected to the implanted layer by a continuous path.

Masks were also made to enable post-implantation metal rings to be deposited as illustrated by the dashed metal C in Fig. 4. This provision is useful for distinguishing surface conducting paths from subsurface paths.

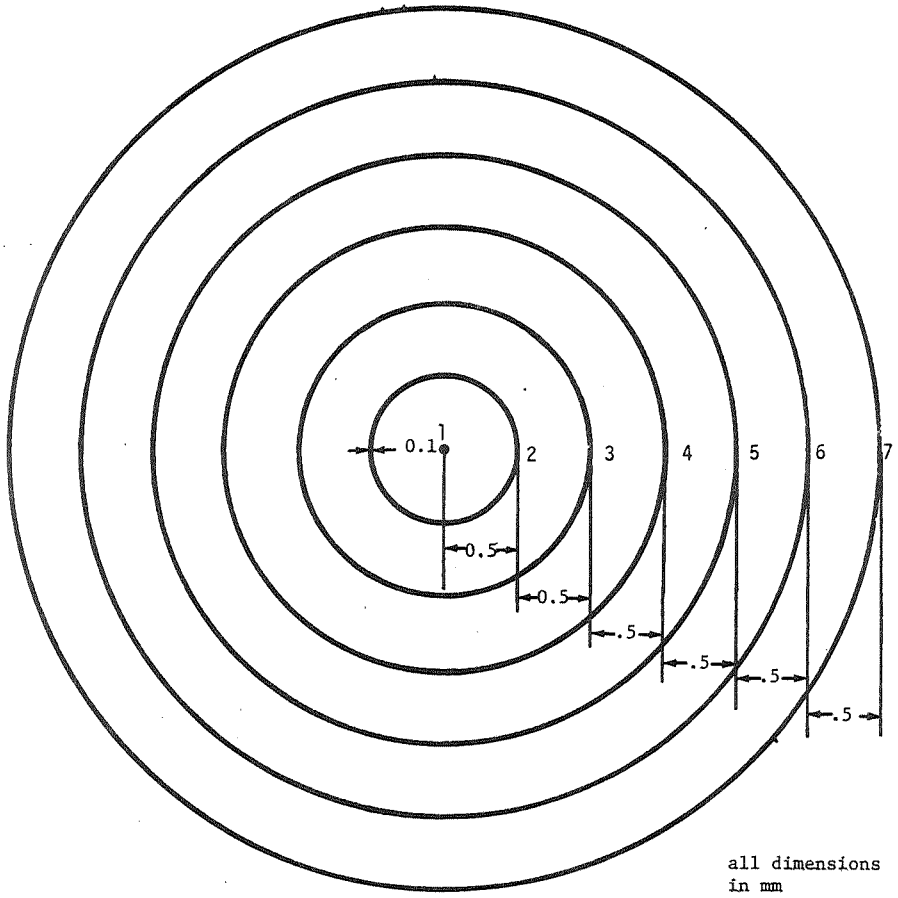

Fig. 3. Surface Geometry

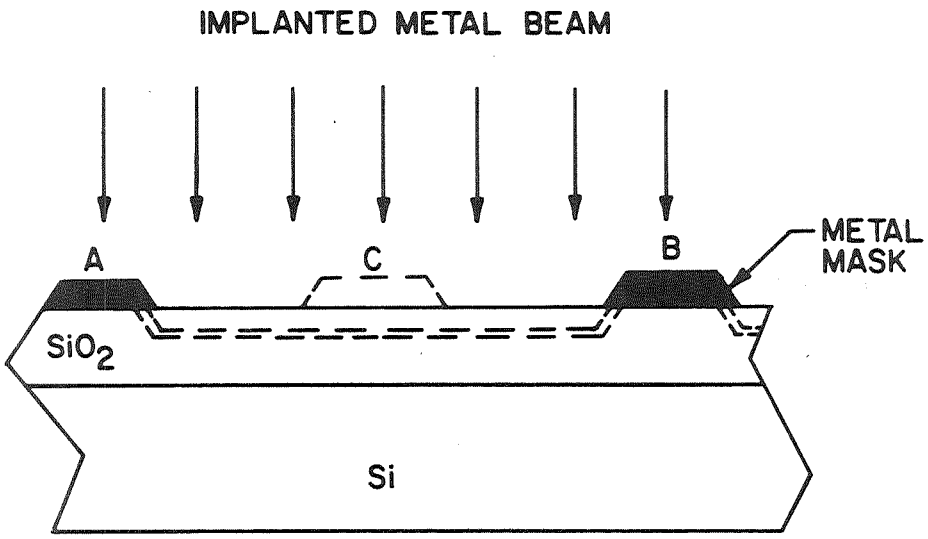

Fig. 4. Implanted profile showing surface contact region.

Ion Implantation

All ion implantations were carried out on the Heavy Ion Source at Langley Research Center. This source is built by Danfysik and at Langley it is coupled directly onto an Ortec electrostatic lens capable of 60 keV acceleration. The beam leaving the accelerator enters a sector magnet for separation and can be post-accelerated through an additional 100 keV before reaching the target. An x-y sweep scans the beam across the desired area in the target chamber. Because of the post-acceleration stage the target chamber is not at ground potential.

The wafers to be implanted were mounted in the target chamber in a fixture shielded by a diaphragm opening of 7/8 inches. The chamber is evacuated by an ion pump to a pressure of 10^{-6} torr or less. The source end of the accelerating column is pumped by a standard oil diffusion pump.

Measurement Methods

Following implantation the wafers were diced and bonded with epoxy to a flat pack; gold wires were bonded to the various rings as shown in Fig. 5. The resistivity of the layers could be measured then by measuring the value of the resistance appearing between any two contacts. The multiplicity of rings and the geometry are suitable for potentiometric measurements if desired.

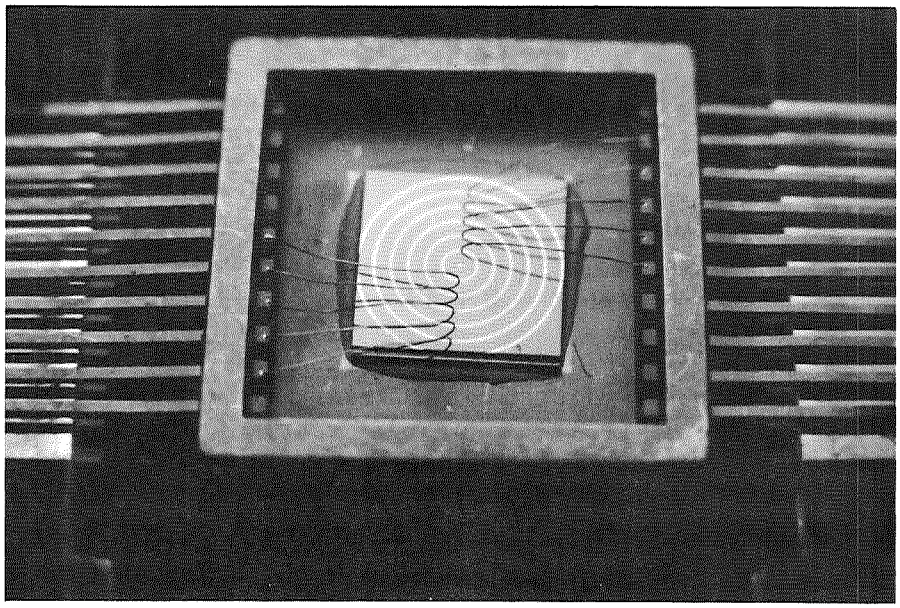

Fig. 5. Mounted and bonded unit ready for test.

Resistance versus temperature measuring technique. - Once the implanted chip is mounted in the flat pack and wire attached between the aluminum rings and the leads of the package, the package can be mounted on a printed circuit board. The printed circuit board couples into a standard PC connector to which appropriate hook-up wires can be soldered. This printed circuit board and connector fit nicely within the Delta MK 2800 temperature chamber which was used to control the temperature during the measurement of resistance. It ranges in temperature between 300°C and approximately -100°C. The resistance of the units under test was determined by measuring the voltage drop across a small known resistor placed in series with the test resistor. A dc voltage between 20 and 100 V was typically impressed across the series combination. This simple arrangement was capable of measuring resistances up to 10^8 ohms. With the contact geometry employed (see the following subsection) the maximum value of sheet resistivity that could be measured was about 5×10^9 ohms/sq. This value was deemed high enough for the purposes of this program.

The current voltage characteristics of the resistors were spot-checked from time-to-time on a Tectronix 575 Curve Tracer. Most resistors appeared linear; those few which did not were removed from the data analysis.

Geometrical analysis. - To convert resistance into values of sheet resistivity requires a solution to the circular contact problem of electrostatics. This problem is handled conventionally by the method of conjugate functions. Consider the circular contacts of Fig. 6a as mathematical functions in the complex plane Z:

$$Z = x + jy = re^{j\theta}. \tag{3}$$

By the logarithmic transformation

$$W = \ell n\ Z = U + jV = \ell n\ r + j\theta \tag{4}$$

circular functions in the Z-plane becomes straight lines in the W-plane as shown in Fig. 6b. The simple rectangular geometry of Fig. 6a is easily solved:

$$R = \frac{\rho \ell}{A} = \frac{\rho}{t}\frac{\ell}{W} = \rho_s \frac{\ell}{W} = \rho_s \frac{U_2 - U_1}{V_2 - V_1}. \tag{5}$$

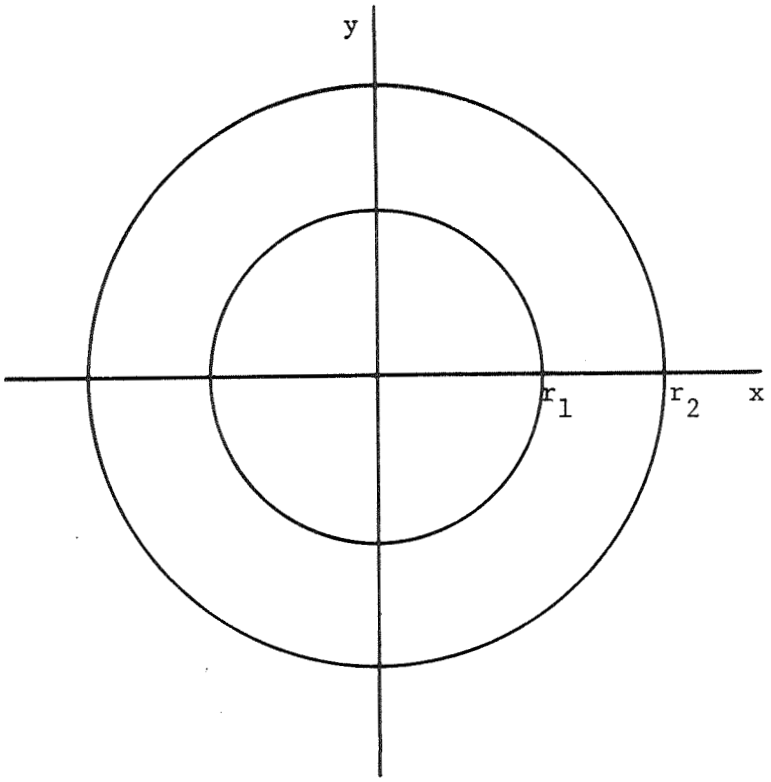

a) Original surface geometry

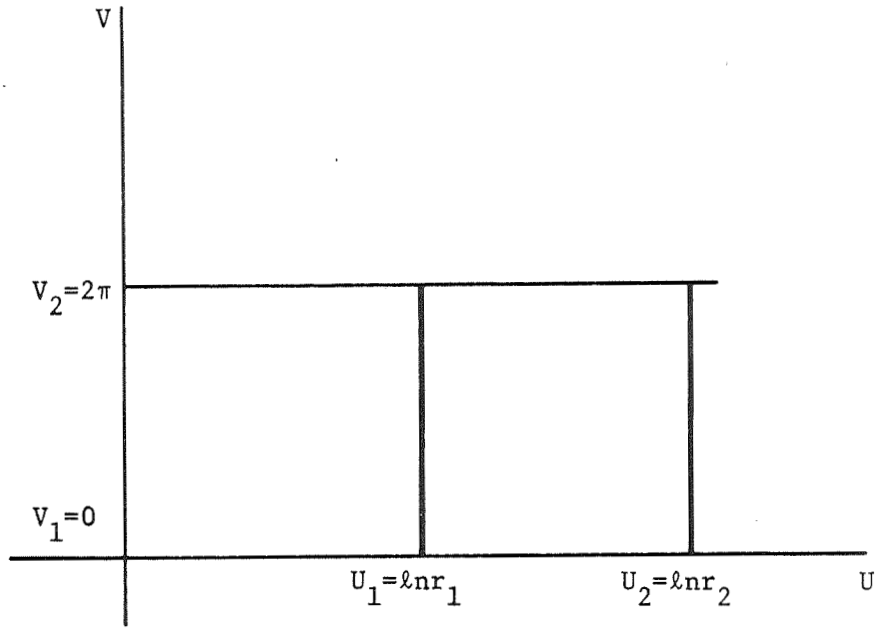

b) Surface geometry following logarithmic transformation

Fig. 6. Conjugate Function Method

Upon substitution of Eq.(4) into Eq.(5), converting the variables of the W-plane back to those of the original Z-plane,

$$R = \rho_s \frac{\ell n \frac{r_2}{r_1}}{2\pi} \tag{6}$$

Equation (6) relates the sheet resistivity, ρ_s, to the measured resistance, R, as a function of the circular contact radii, r_1 and r_2.

Table 1 gives the values of $\ell n \frac{r_2}{r_1}$ relating sheet resistivity and resistance using Eq.(6) and the dimensions of the geometry illustrated in Fig. 3. This table is read by entering the row address with the number of the first contact resistor (see Fig. 3) and proceeding along the column address until the appropriate counter contact is reached; the intersection of the row and column list the value of $\ell n\ r_2/r_1$ to be used in Eq. (6).

Table 1. Correction factors for converting resistance measurements into sheet resistivity

Contact Nos.	1	2	3	4	5	6
2	2.10	-----				
3	2.84	0.548	-----			
4	3.25	0.966	0.322	-----		
5	3.54	1.26	0.621	0.234	-----	
6	3.77	1.49	0.850	0.464	0.182	-----
7	3.96	1.67	1.03	0.647	0.365	0.148

Certain regions on the periphery of the wafer are partially implanted and partially not-implanted. This problem is handled by replacing the factor 2π in Eq.(6) with an approximate angle of intersection for the two contacts. For example, if the beam intersects rings 5 and 6 as shown in Fig. 7, Eq.(6) is modified by replacing 2π with $\pi/3$ where this angle is that corresponding approximately to the dashed lines sketched in lightly.

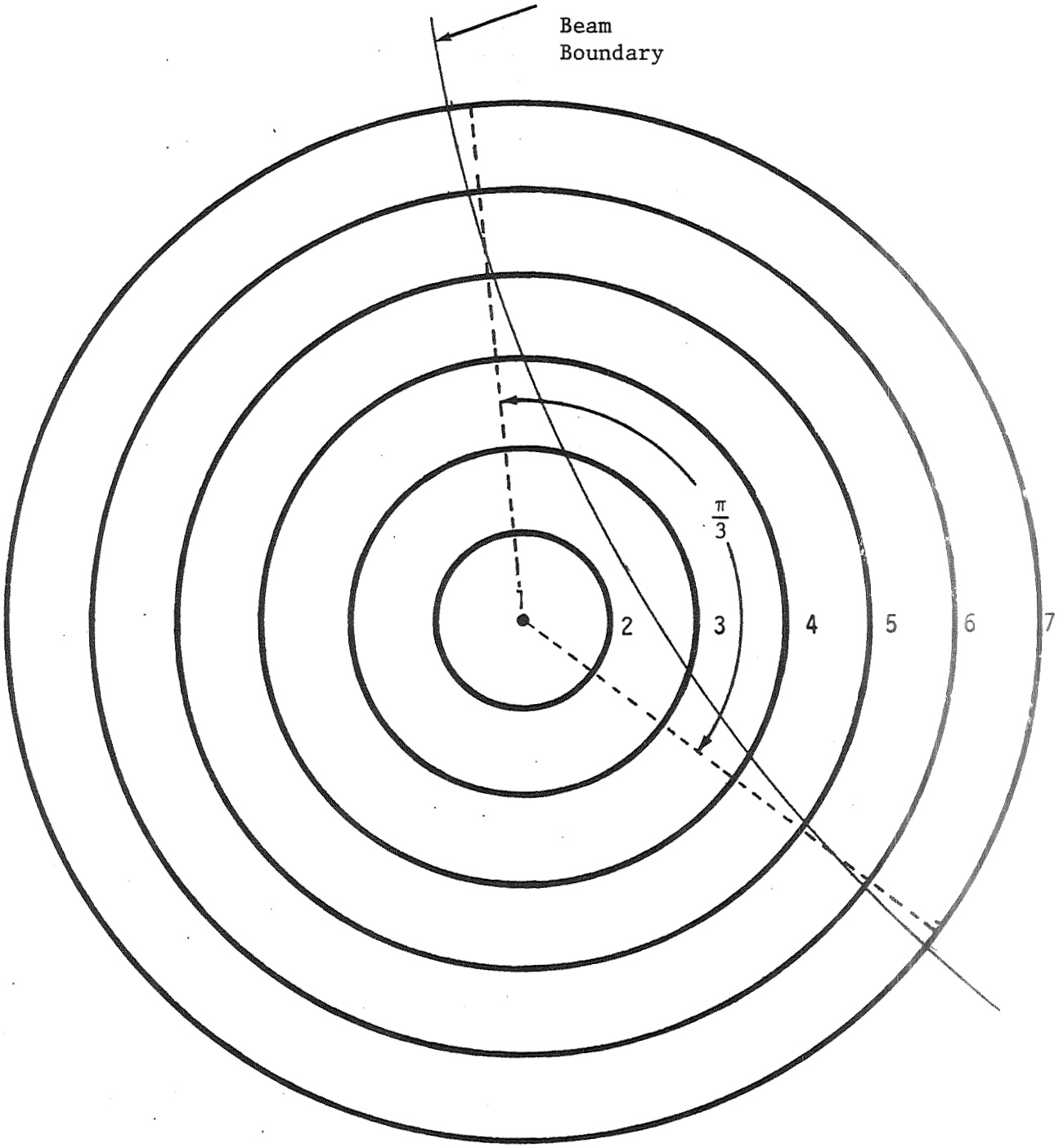

Fig. 7. Approximation Method to Account for Partial Coverage

Problems arose in bonding gold wires to the implanted regions of the aluminum rings and in the early work only peripheral units of the most heavily implanted wafers were used in which the bond was made to a portion of the aluminum ring lying outside the implanted region. The electrical conductivity between any two so contacted rings would still be dominated by the region exposed to the ion beam. The type of correction illustrated in Fig. 7 was necessary in calculating the sheet resistivity from measurements of resistance made on such units.

Annealing Technique

Annealing of the implanted layer is expected to have a major influence on the properties of the implanted layer because of impurity redistribution and diffusion and because of further chemical interaction between the implanted region and the host lattice. Consequently, the initial room temperature data taken on the implanted layers could well vary significantly from that taken after a 300 or 400°C anneal, for example. Consequently, the initial bonding was done as a room temperature process effectively by utilizing a Hughes heated wedge unit. This bonder uses no substrate heat but applies a short pulse of power to the capillary feeding the gold wire. This heat pulse is sufficient to create a nail-head bond between the aluminum and the gold wire and yet the surrounding area experiences little temperature rise. These low temperature bonds were made at Langley through the courtesy of J. Siviter, Meteoroid Research Section, Space Technology Division.

Measurements of Sputtering Losses

The method employed for measuring the thickness of layers sputtered away during ion implantation consists of measuring the step height between a surface exposed to the ion beam and an adjacent surface not exposed to the beam. The aluminum ring contacts which mask the beam are a convenient mask for this measurement. Following ion implantation the aluminum rings are etched away and the height of the step between the oxide previously covered by the aluminum and the adjacent oxide region not covered is a measure of the oxide thickness sputtered away during implantation. The step height is measured by conventional interferometry. Coating the entire surface with a reflective metal like aluminum facilitates the formation of multiple interference fringes which are sharply defined and permit measurement to 0.05 to 0.1 of a fringe spacing (150-300 Å).

SECTION III

RESULTS

This section describes the measurements made in the course of the program and the interpretation placed on these measurements.

Parameters of Implantation

The implantations performed during the course of this program are summarized in Table 2. Five different ions have been implanted into the thermal oxide on silicon. Carbon is expected to be non-reactive with silicon dioxide, as is magnesium; aluminum, of course, is reactive with silicon oxide and hence the chemical interaction should differ between these two species. Argon was chosen as a check on some of the initial results of the program and zinc served as a heavy ion later in the program. All of these ions were selected at least partially because of their relatively high yields using the Heavy Ion Source. The fluences employed varied from 6×10^{15} to 2×10^{17} cm^{-2}. Implantations at these doses requires efficient source operation capable of producing a high beam current if the runs are to be done in a practical length of time. Typical initial results are plotted in Figs. 8 and 9 in which the resistivity of various implanted layers is presented as a function of measuring temperature (Fig. 9) and the room temperature resistivity is presented as a function of annealing temperature (Fig. 8).

The annealing data are relatively straightforward in that the layer undergoes no major change until the temperature of 550-600°C is reached at which point the resistivity decreases dramatically. This temperature is viewed as that at which the aluminum penetrates through the oxide and makes contact to the underlying substrate as illustrated in Fig. 10. The properties then dominating the resistor are those of the substrate silicon. This action was observed whether the implanted beam had struck the surface or not, and a similar plot describes the resistance measured on an non-implanted wafer except that the values of resistance measured prior to annealing at 600°C are immeasurably high.

The behavior of resistivity versus measuring temperature curves shows a negative temperature coefficient of resistance after low temperature of annealing and a positive temperature coefficient of resistance after the 600°C anneal. This positive temperature coefficient corresponds to that of the substrate silicon in the vicinity of room temperature. (Silicon normally has a negative TCR except around room temperature where the mobility dominates the temperature behavior).

Table 2. Summary of implantations

Wafer No.	Ion Implanted	Energy (keV)	Dose (cm^{-2})	LSS $\overline{R_p}$ (μm)	LSS $\overline{\Delta R_p}$ (μm)	Calculated (via Eq. 1) N_{max} (cm^{-3})	Calculated Nearest Neighbor Separation at $\overline{R_p}$ (Å)
1	C^+	140	2×10^{16}	0.350	0.064	1.3×10^{21}	9.2
2	"	"	"	"	"	"	"
3	"	"	2×10^{17}	"	"	1.3×10^{22}	4.3
4	"	"	"	"	"	"	"
5	Al^+	"	6.35×10^{15}	0.165	0.036	7.1×10^{20}	11.2
6	"	"	"	"	"	"	"
7	"	"	6.35×10^{16}	"	"	7.1×10^{21}	5.2
8	"	"	"	"	"	"	"
9	Mg^+	"	1×10^{17}	0.175	0.037	1.1×10^{22}	4.5
10	"	"	1×10^{16}	"	"	1.1×10^{21}	9.7
17	Ar^+	120	1×10^{17}	0.097	0.021	1.9×10^{22}	3.8
18	Ar^+	120	1×10^{17}	"	"	"	"
19	Mg^+	120	1×10^{17}	0.150	0.033	1.2×10^{22}	4.4
20	Mg^+	140	1×10^{17}	0.175	0.037	1.1×10^{22}	4.5
	"	77	6×10^{16}	0.095	0.023	1.0×10^{22}	4.6
	"	41	4×10^{16}	0.052	0.013	1.2×10^{22}	4.4
	"	22	2×10^{16}	0.029	0.007	1.1×10^{22}	4.5
21	Zn^+	60	1×10^{17}	0.032	0.006	6.7×10^{22}	2.5

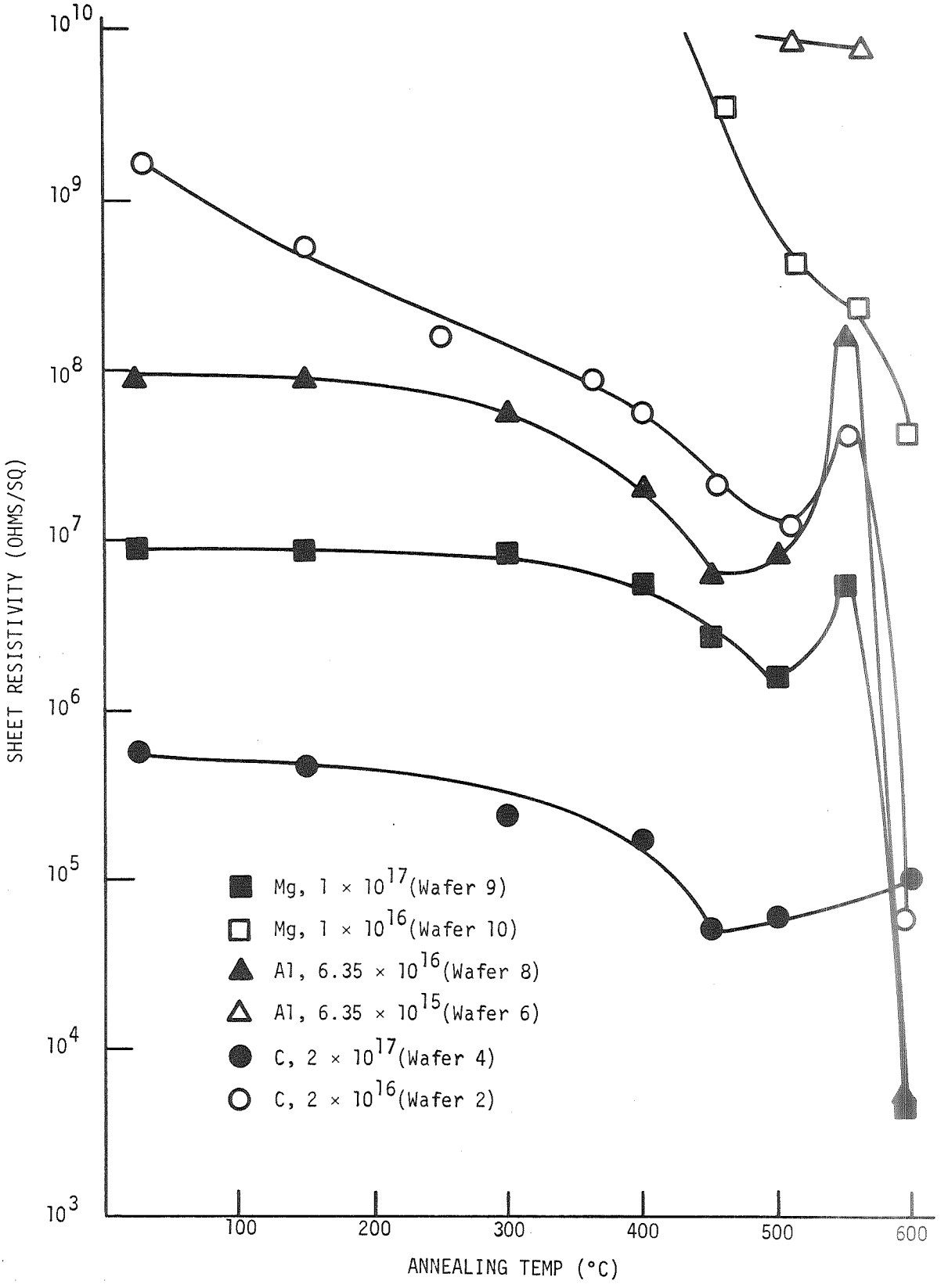

Fig. 8. Probe Measurements of the Annealing Behavior of Various Implanted Layers in Oxide Glass

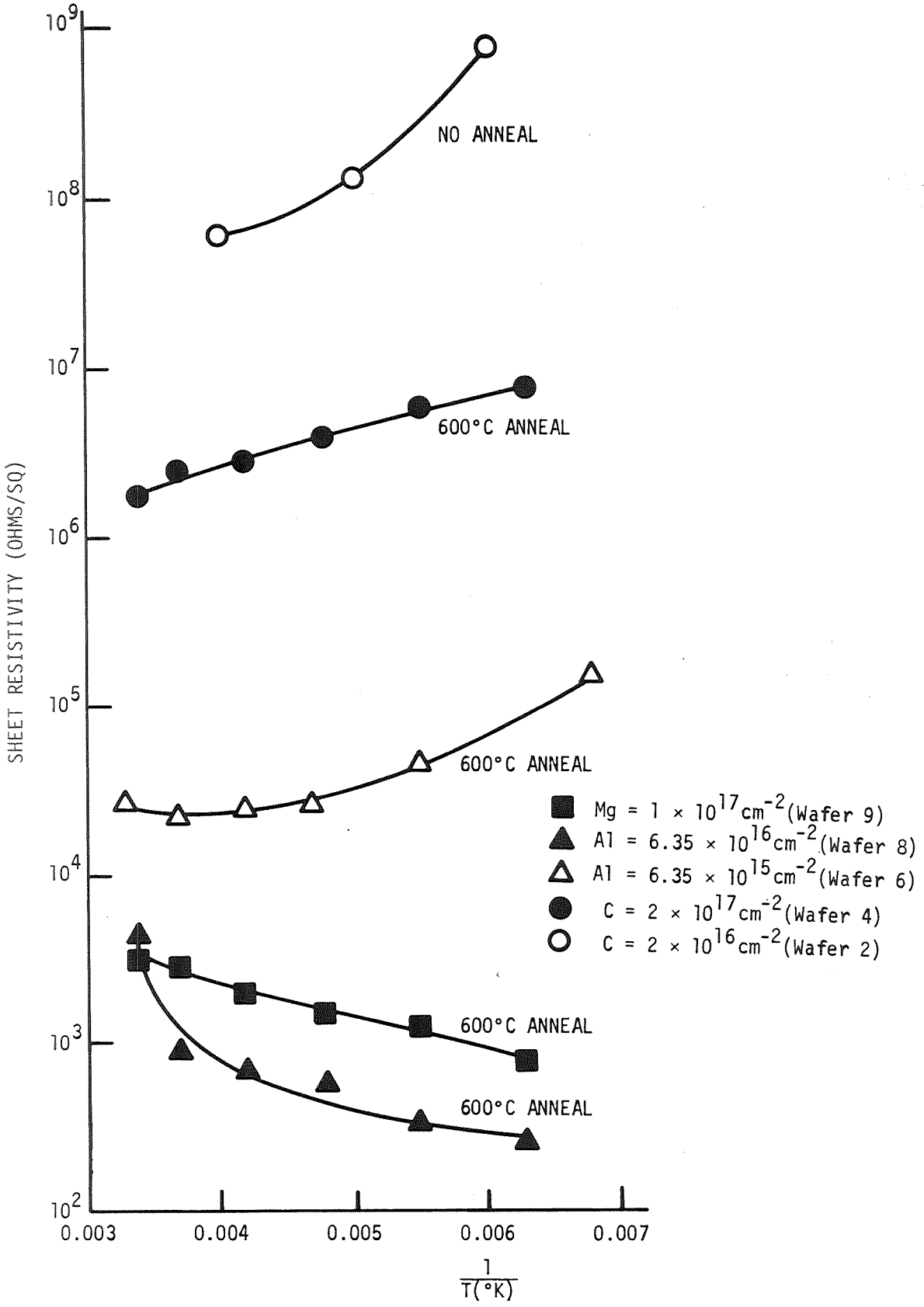

Fig. 9. Change in the Sign of the TCR Brought About By 600°C Annealing

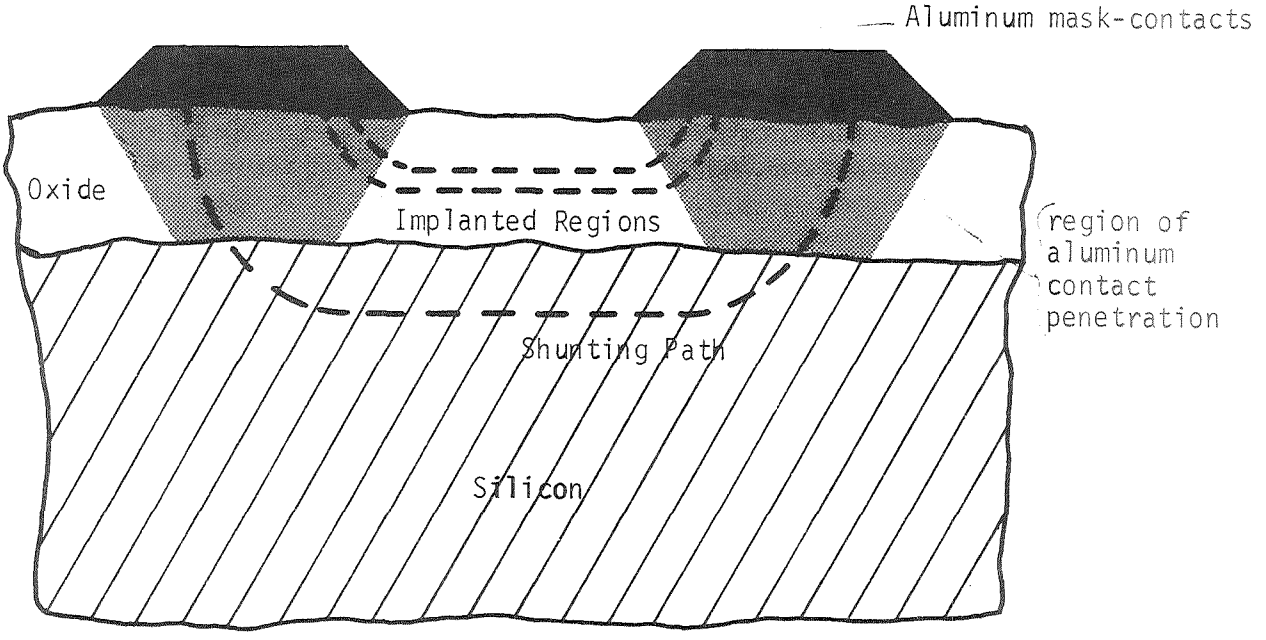

Fig. 10. Shunting path through the oxide and substrate silicon, following 600°C annealing

So far so good, but the most disturbing bit of information was that observed with Implantation 11 in which the implanted species was argon. If the measurements are dominated by the implanted metal species, the expectation is that argon implantation would produce no effect and one would expect that the resistors following Ar^+-implantation would behave much like the unimplanted resistors previously mentioned. This is not the case. The resistance behaved very similar to those shown in Fig. 8 and 9 following ion implantation with argon. This conflicts with the presumed model of the metal-implanted resistors and seriously questions the source of resistance being observed.

Subsequent cleaning experiments in which an attempt was made to remove any surface deposits by exposing the wafer to a plasma cleaning operation removed the resistance measured on all samples implanted. The plasma cleaning operation employed a low temperature asher, LTA 600, manufactured by Tracerlabs, Inc. The unit operated at 300 W using 100% oxygen as the charging gas. Exposure was generally 15 minutes which was sufficient to eliminate the resistance in all cases but one. This was sample 20 on which multiple, high-dose implants had been carried out. Repeated exposure to the plasma cleaning did not completely eliminate the resistor and the surface retained a sufficiently discolored appearance so that the outline of the implanted area remained visible even after 45 minutes of plasma

cleaning. This suggests that there is a surface deposit on the wafer following ion implantation which is generally removed by a plasma cleaning step. The wire bonding difficulties previously cited are also consistent with the presence of a surface film prior to plasma cleaning. After plasma cleaning, the aluminum contacts are no longer discolored and are easily wire bonded. There is a limit to the efficiency of the plasma cleaning as illustrated by Wafer 20 in which the extraordinarily high dose built up a film which was not completely removed even by a much longer exposure to the oxygen plasma.

The source of this film is not known. The initial suspicion was that it was photoresist residue which interacted with the ion beam to form a tough, conducting, but relatively insoluble film. Wafers were prepared in which the photoresist was removed using the plasma cleaning step prior to exposure to the ion beam (Wafers 18 to 21). But again the resistance following implantation was similar in magnitude and independent of implanted species as before. And again a post-implantation plasma cleaning eliminated the resistor and removed the surface stain outlining the beam position on the wafer.

This film does not exist where the beam does not hit. The residue may or may not be on the surface prior to insertion into the ion implantation machine, but it seems clear that an interaction with the beam is necessary in order to create this conducting film.

Consequently, the interpretation of the data pictured in Figs. 8 and 9 is that two different paths of current flow are responsible for the observations. Path 1 is a conducting film across the surface of the wafer connecting one contact with the second. The data presented in Fig. 9 correlate Path 1 more with total dose of implantation than the species or energy or any other factor of the implantation process; that is, the lowest resistance is measured on the heaviest dose of implantation and the highest resistance is measured on the lightest dose of implantation. This observation supports the existence of a surface layer whose magnitude depends upon the dose. It seems unrelated to the species being implanted, the energy of implantation, or any other identifiable variable other than total integrated beam current (implanted charge).

Path 2 is that observed after high temperature annealing and constitutes a current flow through the oxide and the silicon to the other contact. Significantly neither of these paths is the conducting path we set out to investigate--that of the subsurface implanted layer within the oxide. The question remains then, why do we not see the properties of this implanted layer following the removal of the shunting surface path with the plasma cleaning step?

One possibility is that the plasma cleaning is in fact sputtering away the entire implanted region. This possibility was investigated by measuring the amount of oxide removed in a typical plasma cleaning. This was

done by a standard interference fringe technique and revealed that 200 Å of oxide at most is removed during the implantation and plasma cleaning step. This value was arrived at simply by removing the aluminum rings that were in place during implantation and checking for an oxide step at the position where the rings were (see Sec. 2, p. 12). At most a 200 Å step existed. The $\bar{R}_p$ of all implanted layers investigated was far greater than this modest number and consequently the hypothesis that the plasma cleaning is removing the implanted layer is refuted.

Additional evidence that sputtering during plasma cleaning is not significant can be seen by comparing Wafer 20 with all other plasma cleaned wafers. Wafer 20 had multiple energy implants at roughly the same fluence, but the total dose was 2-4 times greater than that on any other sample. Even with repeated cleaning in the plasma oxidation apparatus the post-implantation resistor could not be completely removed (unlike all other wafers studied). Since the extra implantations made on this wafer were all lower energy implantations than those made on the other wafers, the depth of the resistor should be no greater than on these other wafers. If sputtering were the chief cleaning interaction and the layers sputtered away included the implanted resistor, then certainly this layer should have been removed as rapidly on Wafer 20 as on all other wafers. The fact that this could not be done suggests that it is a tough, hard-to-remove surface film that is forming the resistor and that the cleaning action of the plasma, which is chiefly chemical, is not able to remove the thicker surface film from Wafer 20 as completely as with the other less heavily implanted wafers.

Two other possibilities suggest themselves to account for the failure to observe the electrical properties of the implanted layers:

(1) the ions are not ending up where they are assumed to;

(2) they're interacting with the oxide in all cases to form a new insulating compound, such as mullite ($3Al_2O_3 \cdot 2SiO_2$) or forsterite ($2MgO \cdot SiO_2$), both of which are common ceramics.

The first hypothesis can be checked by two experiments as follows:

(1) Carry out the implantation and measurements at liquid nitrogen temperature. If the implanted impurity is not ending up in the distribution that LSS theory predicts, it may be aggregating in precipitates or diffusion to much greater depths than forecast. Carrying out both implantation and measurements at low temperature is expected to slow down both processes. Consequently, effects that have disappeared during room temperature implantation and/or storage might be observed at liquid nitrogen temperature.

(2) Alternatively one could select an ion for implantation which would be easy to profile both by backscattering surface measurements and nuclear counting as well as optical absorption and electron microscopy. Such an ion is mercury. Mercury can be counted relatively easily by neutron activation. The recommended experiment is to implant mercury in much the same energy and density as those previously implanted elements and then, by backscattering, neutron activation and various optical or microscopic methods, determine its location within the oxide. Backscattering and neutron activation examine depth only. Transmission electron microscopy can be used to examine lateral distribution and to detect clusters or aggregates if they exist.

Neither of these experiments has been carried out, although Wafer 21 was implanted at -130°C. Interestingly the surface film dominating the measurements of all other wafers was absent on Wafer 21. Apparently low temperature implantation reduces or eliminates the surface deposit. The question of what happened to the implanted metal is still not answered, however.

The existence of independent evidence that ion implanted layers can be made to exhibit electrical properties in oxide glass does exist [Ref. 4]. This knowledge makes one favor hypothesis (2) in seeking to explain the lack of electrical conduction of the layers implanted in this program. In Reference 4 a brief mention is made of a semiconductor produced by implanting 40 kV Ir ions into "several oxide glasses". Presumably other similar metals such as platinum or osmium could be made to behave similarly. Again an important criterion for selecting the metal to be implanted is the availability of a high yield source.

Another possible explanation for the failure to observe conductivity is that the implanted beam fails to make contact with the aluminum masking rings. For example, in the plasma cleaning step, the removal of the post-implantation resistor following plasma cleaning might simply be a breaking of the contact between the edge of the metal and the implanted region. On one sample, the two adjacent rings were protected by an additional wax deposit placed on top of the rings, but not extending from one ring to the other. An oxide region centered between the two rings was left uncovered. On another set of rings the wax was extended from one adjacent ring to the next. Following the standard 15-minute plasma cleaning step, the resistor between the first two rings, those which were not joined by the wax mask, was broken as before. The two rings that were joined by a continous wax mask still exhibited a conducting path. This experiment shows that the conducting path can be broken at points other than the junction between the aluminum and the implanted layer and that the existence of a weak link at this junction is not a necessary condition for the removal of the conducting path.

In a second experiment designed to check the metal to implanted layer contact the implanted oxide was etched in two steps with aluminum being deposited after each step. The first step consisted of the removal of

0.13 μm of oxide followed by an aluminum deposition. The second step was a repeat of the first with a fresh aluminum deposition. The idea was to contact the implanted layer closer to its maximum concentration. In both cases this attempt failed--no measurable conduction could be observed after either step removal. This particular sample was Wafer 4, the unit implanted at 2×10^{17} C^{+} cm^{-2}.

SECTION IV

CONCLUSIONS

Five different ions have been implanted into glassy silicon oxide layers thermally grown on polished silicon substrates. Four of these ions were elements which in bulk form are good conductors of electricity. The fifth element was argon. Even though the dose and predicted distribution of these implanted ions in the oxide layer was such as to create a subsurface layer with atomic density exceeding 20 percent that of the host lattice, no electrical conduction through these layers could be measured. Various other conducting paths were identified, both after implantation and after high-temperature annealing, but current flow through the implanted layer was not observed.

Of the various explanations hypothesized to explain this lack of conduction two are viewed as the most likely:

(1) the implanted ions are not in the predicted distribution, either laterally, in depth, or both;

(2) the implanted species react with the host oxide to form the non-conducting ceramic phase or compound.

Hypothesis (1) can be checked relatively easily by straightforward profiling and layer scanning techniques. If the distribution is not what is predicted, it is extremely important to determine these parameters. If, however, the impurities are found to be distributed in a profile similar to that predicted, then the second hypothesis becomes the more likely. This hypothesis can be checked by a two-step experiment in which the composition and structure of the existing subsurface layers are first analyzed. If the existence of a new phase with non-conducting properties is confirmed, the second step is to search out a suitable non-interacting but conducting species for implantation.

REFERENCES

1. J. Lindhard, M. Scharff and H. E. Schiott, "Range Concepts and Heavy Ion Ranges", Dan. Vid. Selsk. Mat. Fys. Medd. 33, 1963.

2. J. F. Gibbons, "Ion Implantation in Semiconductors--Part 1: Range Distribution Theory and Experiments", Proc. IEEE 56, 1968, pp. 295-319.

3. W. S. Johnson and J. F. Gibbons, Projected Range Statistics in Semiconductors, Stanford Univ. Bookstore, Stanford, Calif., 1969.

4. C. C. Sartain, W. D. Ryden and A. W. Lawson, "Semiconductors Produced by Doping Oxide-Glasses with Ir, Pd, Rh or Ru", J. Non-Crystal. Solids 4, 1970, p. 231.